The Astrophysical Journal, 723:993–1005, 2010 November 10 doi:10.1088/0004-637X/723/2/993

THE SPATIAL EXTENT OF (U)LIRGs IN THE MID-INFRARED. I. THE CONTINUUM EMISSION

T. Díaz-Santos[1], V. Charmandaris[1,2,3], L. Armus[4], A. O. Petric[4], J. H. Howell[4], E. J. Murphy[4], J. M. Mazzarella[5], S. Veilleux[6], G. Bothun[7], H. Inami[4], P. N. Appleton[8], A. S. Evans[9], S. Haan[4], J. A. Marshall[4], D. B. Sanders[10], S. Stierwalt[4], and J. A. Surace[4]

[1] Department of Physics, University of Crete, GR-71003, Heraklion, Greece; tanio@physics.uoc.gr
[2] IESL/Foundation for Research and Technology-Hellas, GR-71110, Heraklion, Greece
[3] Chercheur Associé, Observatoire de Paris, F-75014 Paris, France
[4] Spitzer Science Center, Caltech, MS 220-6, Pasadena, CA 91125, USA
[5] Infrared Processing and Analysis Center, MS 100-22, California Institute of Technology, Pasadena, CA 91125, USA
[6] Department of Physics and Astronomy, University of New York at Stony Brook, NY 11794-3800, USA
[7] Department of Physics, University of Oregon, Eugene, OR 97403, USA
[8] NASA Herschel Science Center, IPAC, MS 100-22, Caltech, Pasadena, CA 91125, USA
[9] Department of Astronomy, 530 McCormick Road, University of Virginia, Charlottesville, VA 22904, USA
[10] Institute for Astronomy, University of Hawaii, 2680 Woodlawn Drive, Honolulu, HI 96822, USA
Received 2010 April 21; accepted 2010 August 29; published 2010 October 18

ABSTRACT

We present an analysis of the extended mid-infrared (MIR) emission of the Great Observatories All-Sky LIRG Survey sample based on 5–15 μm low-resolution spectra obtained with the Infrared Spectrograph on *Spitzer*. We calculate the fraction of extended emission (FEE) as a function of wavelength for the galaxies in the sample, FEE_λ, defined as the fraction of the emission which originates outside of the unresolved component of a source at a given distance. We find that the FEE_λ varies from one galaxy to another, but we can identify three general types of FEE_λ: one where FEE_λ is constant, one where features due to emission lines and polycyclic aromatic hydrocarbons appear more extended than the continuum, and a third which is characteristic of sources with deep silicate absorption at 9.7 μm. More than 30% of the galaxies have a median FEE_λ larger than 0.5, implying that at least half of their MIR emission is extended. Luminous Infrared Galaxies (LIRGs) display a wide range of FEE in their warm dust continuum ($0 \lesssim \mathrm{FEE}_{13.2\,\mu\mathrm{m}} \lesssim 0.85$). The large values of $\mathrm{FEE}_{13.2\,\mu\mathrm{m}}$ that we find in many LIRGs suggest that the extended component of their MIR continuum emission originates in scales up to 10 kpc and may contribute as much as the nuclear region to their total MIR luminosity. The mean size of the LIRG cores at 13.2 μm is 2.6 kpc. However, once the IR luminosity of the systems reaches the threshold of $L_{\mathrm{IR}} \sim 10^{11.8}\,L_\odot$, slightly below the regime of Ultra-luminous Infrared Galaxies (ULIRGs), all sources become clearly more compact, with $\mathrm{FEE}_{13.2\,\mu\mathrm{m}} \lesssim 0.2$, and their cores are unresolved. Our estimated upper limit for the core size of ULIRGs is less than 1.5 kpc. Furthermore, our analysis indicates that the compactness of systems with $L_{\mathrm{IR}} \gtrsim 10^{11.25}\,L_\odot$ strongly increases in those classified as mergers in their final stage of interaction. The $\mathrm{FEE}_{13.2\,\mu\mathrm{m}}$ is also related to the contribution of an active galactic nucleus (AGN) to the MIR emission. Galaxies which are more AGN dominated are less extended, independently of their L_{IR}. We finally find that the extent of the MIR continuum emission is correlated with the far-IR *IRAS* $\log(f_{60\,\mu\mathrm{m}}/f_{100\,\mu\mathrm{m}})$ color. This enables us to place a lower limit to the area in a galaxy from where the cold dust emission may originate, a prediction which can be tested soon with the *Herschel Space Telescope*.

Key words: galaxies: active – galaxies: evolution – galaxies: interactions – galaxies: starburst – infrared: galaxies

Online-only material: color figures, machine-readable table

1. INTRODUCTION

The discovery by the *Infrared Astronomical Satellite* (*IRAS*) of luminous and ultra-luminous infrared (IR) galaxies, the so-called Luminous Infrared Galaxies (LIRGs) and Ultra-luminous Infrared Galaxies (ULIRGs),[11] has opened a new window in extragalactic astrophysics. Over the past 25 years, follow-up ground-based and space-born observations of these optically faint systems (see Houck et al. 1984) have revealed much about their detailed physical properties as well as their contribution to the integrated energy production in the universe (see Sanders & Mirabel 1996, and references therein). More specifically, it has been shown that even though LIRGs and ULIRGs are not very common in the local universe (Soifer & Neugebauer 1991), they contribute a substantial fraction of the energy at $z \sim 1$–2 (Pérez-González et al. 2005; Le Floc'h et al. 2005; Caputi et al. 2007). Furthermore, the more IR luminous systems tend to be more disturbed dynamically, show evidence of merging, and often harbor an active galactic nucleus (AGN). The leap in sensitivity provided by the *Spitzer Space Telescope* (Werner et al. 2004) and in particular the availability of deep mid-infrared (MIR) spectroscopy with the Infrared Spectrograph (IRS; Houck et al. 2004) enabled the detailed study of the properties of large nearby (i.e., Armus et al. 2007; Desai et al. 2007; Imanishi et al. 2008; Pereira-Santaella et al. 2010) and more distant (Houck et al. 2005; Yan et al. 2005, 2007) samples of (U)LIRGs. It thus became evident that, given the diversity of the MIR spectra of LIRGs and even more of ULIRGs, these systems cannot be grouped in a common class of galaxies either in terms of their MIR and/or far-infrared (FIR) properties. A number of correlations between the MIR colors, strength of features due to polycyclic aromatic hydrocarbons (PAHs), and line emissions, with the dominant source of energy production or interaction stage of galaxies have been explored (Armus et al. 2007; Desai

[11] LIRGs are defined as systems displaying an IR luminosity, L_{IR}, of $10^{11}\,L_\odot \leqslant L_{\mathrm{IR}[8-1000\,\mu\mathrm{m}]} < 10^{12}\,L_\odot$; ULIRGs: $L_{\mathrm{IR}[8-1000\,\mu\mathrm{m}]} \geqslant 10^{12}\,L_\odot$.

et al. 2007; Veilleux et al. 2009; Petric et al. 2010). It appears that systems which are AGN dominated show weak PAH features, which are also correlated with the FIR spectral slope. Systems with greater MIR luminosity display weaker PAH emission, while dust extinction, quantified by the 9.7 μm silicate feature, varies in strength and does not correlate with starburst or AGN-dominated systems.

Recently, some studies have suggested that $z \sim 2$ ULIRGs are not just the analogs of local ULIRGs but instead they display MIR spectral features more similar to those seen in local, lower luminosity starburst galaxies and LIRGs (Rigby et al. 2008). Some high-z sub-millimeter galaxies (SMGs) with IR luminosities similar to or greater than ULIRGs also show IR properties different from those of local ULIRGs (Pope et al. 2008; Murphy et al. 2009; Menéndez-Delmestre et al. 2009). All this evidence, in combination with results obtained from spatially resolved Hα imaging and CO and radio maps of SMGs, suggests that the star formation (SF) taking place in ULIRGs and some SMGs at high redshift may be occurring over large areas, extending over several kpc across their disks (Bothwell et al. 2010; Ivison et al. 2010; Alexander et al. 2010). This is in contrast to what is seen in local ULIRGs where the strong bursts of SF are concentrated within the central kpc of galaxies probably due to interactions and mergers (Sanders & Mirabel 1996; Downes & Solomon 1998; Bryant & Scoville 1999; Soifer et al. 2000), which efficiently drive gas and dust toward their nuclei.

Here, we present the first part of an analysis which has as the main goal to quantify the amount of extended MIR emission as a function of wavelength of a large sample of local LIRGs and ULIRGs which can be spatially resolved with *Spitzer*/IRS. This will provide extra evidence on the issue of whether the SF observed in high-redshift ultra-luminous systems has the same MIR characteristics as those observed in disks of lower IR luminosity local systems and it will allow us to examine whether the high-z systems are scaled-up versions in size, SF efficiency, and therefore in IR luminosity of local LIRGs or ULIRGs. In this first paper, we study how the extended MIR *continuum* emission relates to global properties, such as the IR luminosity, AGN fraction, merging state, and FIR colors of the galaxies, and derive general trends for the entire sample. In a forthcoming paper (T. Díaz-Santos et al. 2011, in preparation), we will address how the extended emission (EE) varies as a function of other 5–15 μm features, such as PAHs and emission lines, and how it is linked to the particular physical properties of each galaxy.

The paper is structured as follows: In Section 2, we present our sample, the data reduction, and a summary of the analysis we performed in order to calculate the FEE as a function of wavelength for each source. In Section 3, we explore possible correlations of the FEE at 13.2 μm and the IR luminosity, stage of interaction, AGN strength, and FIR colors for our sample, and discuss some implications for the high-redshift SMG population. The conclusions are presented in Section 4, while in the Appendix we provide more details on the analysis of the spatial profiles and the various tests performed in order to ascertain its robustness.

2. OBSERVATIONS AND DATA ANALYSIS

2.1. The Sample

The sample on which we base our analysis is the Great Observatories All-Sky LIRG Survey (GOALS; Armus et al. 2009). GOALS comprises a complete, flux-limited sample of galaxies in the local universe drawn from the Revised Bright Galaxy Sample (RBGS; Sanders et al. 2003) selected to be systems in the (U)LIRG luminosity class. Armus et al. (2009) describe in detail the characteristics of the GOALS sample and Petric et al. (2010) present a comprehensive statistical analysis of the MIR spectral features as probed with *Spitzer*/IRS. Using a number of MIR diagnostics, Petric et al. (2010) estimate the AGN contribution to the MIR luminosity of the systems and, based on their apparent morphology, classify each galaxy into a stage of interaction (from isolated systems to advanced mergers). *Hubble Space Telescope* (*HST*) high spatial resolution optical and near-IR imaging for a fraction of the GOALS sample are presented by Haan et al. (2010). We refer the reader to these papers for further details. Out of the 291 galaxies (202 systems) included in the GOALS sample (see Armus et al. 2009), a total of 221 are used for this study. This is the number of *individual* galaxies for which IRS staring observations are available. Figure 1(a) presents the distribution of the galaxies as a function of their IR luminosity while Figure 1(b) shows it as a function of the distance. For reference, on the right panel we also indicate the projected linear scales that can be resolved at a given distance at 13.2 μm using the IRS 5–15 μm spectra.

The total IR luminosities of our systems were calculated using their *IRAS* flux densities and luminosity distances (see Armus et al. 2009, for details on the cosmology adopted), and following the prescription described in Sanders & Mirabel (1996). Since the spatial resolution of *Spitzer* is much higher than that of *IRAS*, there are MIPS 24 μm *Spitzer* fluxes for 99 individual galaxies within multiple systems. For these, we distributed the $L_{\rm IR}$ of the system among the galaxies proportionally to their 24 μm flux. For those systems without 24 μm measurements of individual galaxies, the $L_{\rm IR}$ was evenly distributed among the members of the system. Due to this redistribution of the $L_{\rm IR}$, there are now 35 galaxies with IR luminosities lower than $10^{11}\ L_{\odot}$ in our sample (see Figure 1(a)). In Table 1, we present the final $L_{\rm IR}$ and distance of the galaxies.

2.2. Spitzer/IRS Observations

All galaxies in GOALS have been observed in staring and/or mapping mode with the *Spitzer*/IRS instrument using all instrument modules (SL, LL, SH, and LH). They also have IRAC (Fazio et al. 2004) and MIPS (Rieke et al. 2004) imaging observations at all bandpasses (J. M. Mazzarella et al. 2011, in preparation). The analysis presented in this paper is based on IRS SL staring observations covering the 5 to $\sim$15 μm wavelength range with a spectral resolution of $R \sim 60$–130. As mentioned earlier, the aim of the study is to separate and quantify the EE of (U)LIRGs from the contribution of the unresolved nuclear component. Thus, we limit our study to the shortest wavelengths where the spatial resolution of IRS ($\sim$3.″6 at 13.2 μm) is sufficient to separate regions of physical scales that range from 0.22 kpc, at the distance of the closest LIRG ($\sim$12 Mpc), to 7 kpc at $\sim$400 Mpc where the farthest ULIRG of the sample is located (see Figure 1). The median distance of our Galaxy sample is 99 Mpc, at which the spatial resolution is 1.7 kpc (also at 13.2 μm). In order to test the validity of some of the results obtained from the IRS SL spectroscopy, we also used the 8 μm IRAC imaging (see the Appendix and J. M. Mazzarella et al. 2011, in preparation for details).

2.3. Data Reduction

As explained in Petric et al. (2010), all data were reduced using the S15, S16, and S17 IRS pipelines at the Spitzer Science

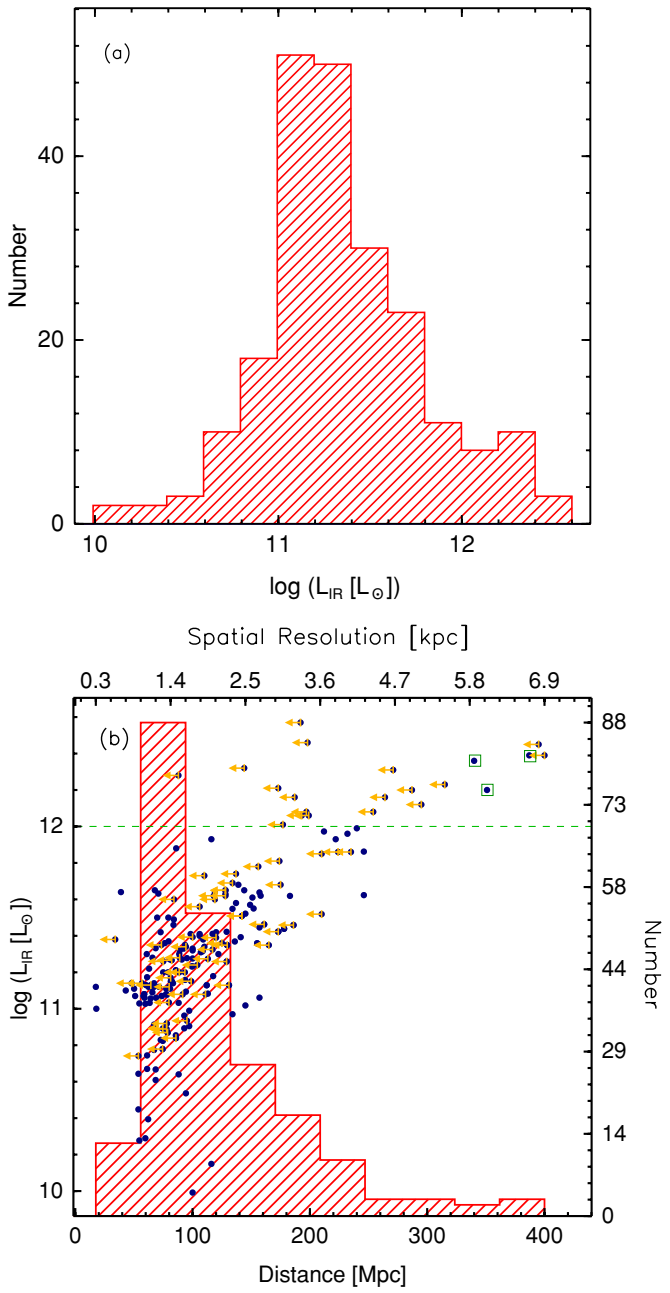

Figure 1. Histograms of the GOALS galaxy sample. (a) Distribution in IR luminosity. (b) Distribution in distance, indicated on the right *y*-axis. The upper *x*-axis displays the projected linear scale that can be resolved at 13.2 μm at a given distance with IRS. The blue dots are the actual data points, with their L_{IR} indicated on the left *y*-axis of the plot. Upper limits in the *x*-axis value of a galaxy imply that its "core" is unresolved (see Section 3.2 and Figure 4). The green dashed line marks the boundary between LIRGs and ULIRGs. Except for three special cases (green boxes; see also Figure 4), all ULIRGs have unresolved cores independently of their distance.

(A color version of this figure is available in the online journal.)

Center.[12] The pipelines were changed to modify certain header keywords, produce new flat-fields, lower SL and LL fringes by 1%–20%, and provide better treatment of ramp slopes. The changes made between the pipelines should not systematically alter the measurements presented here. The reduction includes ramp fitting, dark sky subtraction, droop correction, linearity correction, and wavelength and flux calibration.

[12] See http://ssc.spitzer.caltech.edu/irs

The backgrounds in the high-resolution data were subtracted for all objects with dedicated sky observations (~60% of the sources). For the low-resolution data without dedicated background observations, off-source nods were used for sky subtraction. Large objects in PID 30323 had dedicated background pointings. Bad pixel mask files were combined such that the final masks flagged all the individual bad pixels, if they were marked as bad in one individual exposure. Basic calibrated data sets (BCDs) for each nod were combined by determining the median if more than five BCDs were available, otherwise the average was used with 3σ clipping. Finally, two dimensional coadds for each nod position and SL module were created.

2.4. Analysis

In this subsection, we briefly summarize how, using 5–15 μm *Spitzer*/IRS SL staring observations, we can estimate the FEE of the galaxies as a function of wavelength, FEE_λ. More technical details of our analysis, as well as information on the specific treatment of the IRS data, are provided in the Appendix.

We commence the analysis with the two-dimensional co-added files of the GOALS sample reduced as described above (see Petric et al. 2010). We use the exact algorithms of the SSC pipeline, as well as the grid mapping of the slits on the IRS detector identified by the pseudo-rectangles of the "wavesamp" file to extract the spatial profiles of each source along the slit as a function of wavelength for each order and nod position. We follow the same approach to obtain the spatial profiles of a standard star (HR7341; PID: 1432) that we use as the reference point-spread function (PSF) of an unresolved source.

For each wavelength resolution element, we fit the spatial profiles of the stellar PSF and the galaxy with Gaussian functions in order to calculate their peaks of emission and full width at half-maximums (FWHMs). The FWHM of the Gaussian used to fit the galaxy profile is what we call the galaxy "core" size (see below). We then scale the peak of the spatial profile of the stellar PSF to the maximum of the spatial profile of the galaxy and subtract it. What remains is the spatial profile of the EE of the galaxy at a given wavelength. This EE (EE_λ) divided by the integrated emission of the galaxy all along the slit is what we define as the FEE as a function of wavelength, FEE_λ. We refer the reader to the Appendix for a more detailed explanation on its rather challenging calculation and the corrections that have to be applied to obtain reliable values. So formally

$$\mathrm{FEE}_\lambda = \frac{\mathrm{EE}_\lambda}{E_\lambda(\mathrm{total})}, \quad (1)$$

where FEE_λ, EE_λ, and E_λ(total) are the FEE (ranging from zero to unity), the EE, and the total emission of the galaxy at a given wavelength, respectively. Note that since we are scaling the stellar PSF to the maximum of the spatial profile of the galaxy, we implicitly assume that its nuclear emission is entirely produced by the central unresolved component. Therefore, the values of EE_λ and the FEE_λ calculated in this manner are lower limits to the true EE. We report as the final FEE_λ at a given wavelength the average of the values obtained for each one of the two nod positions of the IRS slits. Comparing the difference between the two nods, we calculate the statistical uncertainty of the FEE_λ. The final uncertainty includes additional sources of error and depends on the details of the target (see the Appendix for more information). For reference, the typical uncertainty on the FEE is between 0.05 and 0.15 (see Table 1).

Since the projection of the IRS slit over the galaxies does not entirely cover the size of the emitting region, we visually

Table 1
Properties of the Sample

Galaxy Name (1)	R.A. (J2000) (2)	Decl. (J2000) (3)	Distance (Mpc) (4)	log L_{IR} ($L_\odot$) (5)	FEE$_{13.2\,\mu m}$ (6)	Core Size (kpc) (7)	*IRAS* log($f_{60\,\mu m}/f_{100\,\mu m}$) (8)
NGC 0023	$00^h09^m53\overset{s}{.}4$	$+25^\circ55^m27^s$	65.2	11.12	0.67 ± 0.03	2.62 ± 0.02	-0.239 ± 0.004
MCG-02-01-051	$00^h18^m50\overset{s}{.}9$	$-10^\circ22^m36^s$	117.5	11.18	0.28 ± 0.06	2.28 ± 0.02	-0.111 ± 0.007
ESO350-IG038	$00^h36^m52\overset{s}{.}5$	$-33^\circ33^m17^s$	89.0	11.28	0.07 ± 0.08	1.57 ± 0.01*	0.135 ± 0.003
NGC 0232	$00^h42^m45\overset{s}{.}8$	$-23^\circ33^m41^s$	95.2	11.28	0.37 ± 0.06	2.09 ± 0.01	...
NGC 0232	$00^h42^m52\overset{s}{.}8$	$-23^\circ32^m27^s$	95.2	10.93	0.15 ± 0.07	1.79 ± 0.01*	...
MCG+12-02-001	$00^h54^m03\overset{s}{.}9$	$+73^\circ05^m05^s$	69.8	11.50	0.42 ± 0.06	1.65 ± 0.01	-0.123 ± 0.006
...	...	...	...	...	...	...	...

Notes. Columns: (1) Galaxy name. Multiple systems are indicated with the same name but providing the right ascension and declination of the individual galaxies. (2) Right ascension (J2000). (3) Declination (J2000). (4) Luminosity distance (see Armus et al. 2009 for details). The L_{IR} is accurate to within 0.01 dex (U et al. 2011, in preparation). (5) IR luminosity of the galaxy (see Section 2.1 for details on its calculation). (6) FEE at 13.2 μm (FEE$_{13.2\,\mu m}$). (7) Size (FWHM) of the galaxy core at 13.2 μm (see the Appendix). The asterisks denote galaxies with unresolved cores (FWHM within 10% of that of the unresolved stellar PSF). The colons indicate galaxies whose IRS spectra have been contaminated by a close companion galaxy. In these cases, the FEE$_{13.2\,\mu m}$ and the core size are not reliable. (8) *IRAS* log($f_{60\,\mu m}/f_{100\,\mu m}$) color. Values are given only for sources with a unique *IRAS* color, i.e., not associated with two individual galaxies.

(This table is available in its entirety in a machine-readable form in the online journal. A portion is shown here for guidance regarding its form and content.)

inspected their corresponding IRAC 8 μm images in order to examine whether the slit was placed systematically along a privilege direction over the disk of the galaxies. We found that, most likely due to the large size of our sample, the position angle of the slit was randomly distributed along different directions on the galaxies and was not oriented systematically along bars, spiral arms, or regions of enhanced SF. As a consequence, variations in the intrinsic inclinations of the disks in more extended systems do not bias our findings.

3. RESULTS

The FEE as a function of wavelength, FEE$_\lambda$, calculated for each one of the sources, contains a wealth of information. In the present section, we discuss the types of FEE$_\lambda$ we typically see in our sample, as well as the properties of the EE in the MIR continuum. For the latter, we use the resolution element at 13.2 μm (FEE$_{13.2\,\mu m}$) as reference, as it is an area of the spectrum which is devoid of known emission or absorption features. Our findings though are similar for the 5–15 μm MIR continuum in general.[13] A detailed comparison of the FEE$_\lambda$ for different MIR spectral features (e.g., PAHs, emission lines, or the 9.7 μm silicate absorption feature) and the correlation of their ratios with the characteristics of each galaxy (e.g., nuclear and total extinction, the presence of an AGN) will be addressed in a companion paper (T. Díaz-Santos et al. 2011, in preparation). In addition, we construct spectra for the nuclear and extended components of galaxies as a function of the FEE$_\lambda$ types. Table 1 presents the FEE$_{13.2\,\mu m}$ values for the galaxies in our sample, their "core" size at the same wavelength (see the previous section and the Appendix), and their *IRAS* log($f_{60\,\mu m}/f_{100\,\mu m}$) ratio, as well as other basic characteristics.

3.1. *Types of* FEE$_\lambda$ *Profiles*

If one ignores projection effects or details on the intrinsic geometry of a source, the spatial profile of a galaxy as a function of wavelength, and consequently the estimated FEE$_\lambda$, depends primarily on the origin of the emission within the galaxy. The MIR continuum emission, PAH features, emission lines, as well as absorption features do not always originate from the same physical regions. Therefore, it is reasonable to expect that the FEE$_\lambda$ function varies among the galaxies. We find three different FEE$_\lambda$ types, whose shapes are similar among the galaxies examined here. We exclude from this study eight sources (4% of the sample) that appear practically unresolved in the 5–15 μm range and for which their FEE$_\lambda$ $\simeq$ 0. We also exclude 11 galaxies (5% of the sample) whose FEE$_\lambda$ could not be classified in any of the three types.

1. *Constant/featureless*. 111 (50%) (U)LIRGs display a constant FEE$_\lambda$ across the whole IRS 5−15 μm wavelength range (see Figure 2, left panel). No MIR feature appears more extended than another or even than the continuum emission. This implies that there is no differentiation in the spatial distribution of the type of emitting region along the IRS slit. These constant FEE$_\lambda$ functions range between ∼0.1 up to ∼0.85 among the galaxies of this type. A representative member of this type is NGC 3110 that, in particular, has a constant FEE$_\lambda$ of ∼0.65.
2. *PAH and line extended*. 37 galaxies (17%) of the sample show MIR features which are clearly more extended than the continuum emission (see Figure 2, central panel). More than ∼20% of the flux detected in several PAH features and emission lines is extended, and in some sources it can be as high as 70%. In these types of galaxies, the bulk of the continuum emission originates from a region more compact than that giving rise to the MIR spectral features. The fact that these two components of emission are spatially decoupled suggests that, contrary to the previous type of FEE$_\lambda$, different physical processes are responsible for the energy production in the nucleus and in the disk. This could be due to the presence of either an AGN or an intense starburst in the nucleus producing a strong MIR continuum, compared to a more quiescent SF on the disk where older stellar populations may heat the gas and PAH molecules. A representative member of this type is NGC 1365.

[13] Note that this does not hold when the emission at ∼24 μm is examined since the slit width of the IRS LL module is 10.″5, nearly three times worse than that of the SL (A. Petric 2010, private communication).

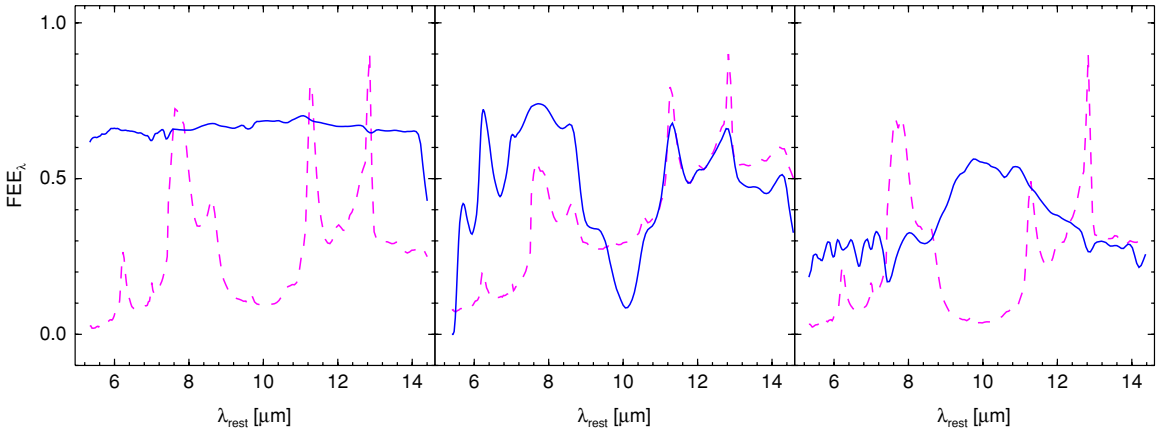

Figure 2. FEE$_\lambda$ function of three galaxies that serve as examples of the three types identified in the sample (blue solid line). The spectrum of each galaxy, scaled to arbitrary units, is also plotted for reference (pink dashed line). The galaxies are NGC 3110 (left), NGC 1365 (center), and MCG+08-11-002 (right). The FEE$_\lambda$ functions have been smoothed with a four-pixel box to reduce the noise. Left panel: constant/featureless FEE$_\lambda$. Middle panel: PAH and line EE. Right panel: silicate EE.

(A color version of this figure is available in the online journal.)

3. *Silicate extended.* Another 54 (24%) galaxies of the sample show a rather interesting FEE$_\lambda$ shape in which the maximum peaks around 10 μm (see Figure 2, right panel). Inspecting the FEE$_\lambda$ closely, it appears that there is an increase between ∼8 and 12 μm, around the wavelength range where the 9.7 μm silicate absorption feature is present. We attribute this maximum to an extinction effect in these systems. Galaxies containing very obscured nuclei will show little or not at all "unresolved emission," at wavelengths dominated by the silicate absorption feature. As mentioned earlier, we always normalize the spatial profile of an unresolved point source to the source profile at every wavelength and subtract it in order to determine the value of FEE$_\lambda$. Consequently, if the nucleus of a galaxy is very extinguished, any residual emission within the 9.7 μm band, when compared to the emission at any other wavelength that is not affected by the absorption feature, would be interpreted as an excess in the FEE originating from the outer disk of these galaxies, where the extinction is less extreme. This is reflected in the form of FEE$_\lambda$ we compute and implies that the silicate strength (i.e., the apparent optical depth) calculated from the integrated spectrum of these galaxies may not be representative of their nuclei (see Spoon et al. 2004). A representative member of this type is MCG+08-11-002.

The presence of these types of FEE$_\lambda$ suggests that the mechanism by which local (U)LIRGs produce the MIR emission in their disks and nuclear regions varies from one source to the next. There is a great diversity not only in the integrated spectrum of an LIRG/ULIRG, but also in the spatial distribution of the regions responsible for the formation of the various MIR features, such as PAHs, emission lines, and dust continuum. The different FEE$_\lambda$ types indicate that in some galaxies the emission from PAHs, atomic, or molecular lines is more extended than the dust continuum emission, while in others their extent is similar. These variations are clearly related to the location and intensity of the physical process producing the emission detected, such as young star clusters or an AGN. Our results suggest that not all local (U)LIRGs are to be a priori considered as compact, uniform MIR emitters. There has been an interesting such case reported already, VV114, a system with $L_{IR} = 4 \times 10^{11}\,L_\odot$ harboring an AGN, for which high-resolution ground-based MIR imaging (Soifer et al. 2001), as well as 5–15 μm ISO/CAM spectral maps reveal that nearly 60% of the MIR emission is extended (Le Floc'h et al. 2002). In these types of systems, the MIR is not necessarily dominated by an AGN or a single burst of SF. Moreover, in the cases of purely starburst-driven (U)LIRGs, the PAH and continuum emission may not be associated with the same SF event but instead are probably excited, as a whole, by different stellar populations. For example, the 11.3 μm PAH emission is more representative of *recent* SF events with ages greater than 8–10 Myr, while *current* SF, less than 8–10 Myr in age, is better traced by the [Ne II]12.81 μm or MIR continuum emission (Díaz-Santos et al. 2010). In these galaxies, older SF traced by PAH emission is more extended and is more typical of galactic disks, while recent SF, associated with MIR continuum emission, is more compact and concentrated toward the nucleus.

3.2. The L_{IR} Dependence of the Extended Emission

The histogram in Figure 3 presents the distribution of the median FEE$_\lambda$, calculated over the whole 5–15 μm range, for all the galaxies in our sample (black histogram). 32% of the galaxies have a median FEE$_\lambda$ larger than 0.5, that is, at least 50% of their MIR is extended. In addition, more than 90% of the galaxies have a median FEE$_\lambda$ larger than 0.1.

High-resolution MIR images of a handful of local (U)LIRGs have revealed rather compact emission originating from a few hundred parsecs around their nuclei (Soifer et al. 2000, 2001; Díaz-Santos et al. 2008). This trend is also present in our data, even though the physical scales we probe with *Spitzer* are larger. In Figure 3, we also show three histograms of the median FEE$_\lambda$ for galaxies grouped in three ranges of IR luminosity. We note that galaxies with $L_{IR} < 10^{11.25}\,L_\odot$ (red histogram) and $10^{11.25}\,L_\odot \leqslant L_{IR} < 10^{12}\,L_\odot$ (orange) display similar median values of their FEE$_\lambda$ distributions. The median of each histogram is 0.46 and 0.39, respectively, which is in agreement with previous studies based on smaller samples of LIRGs (Pereira-Santaella et al. 2010). The median values of the low IR luminosity bins are very similar to that found for the median FEE$_\lambda$ of the whole sample of galaxies, 0.40. However, we find that the median of the corresponding distribution for ULIRGs (blue histogram) is only 0.14. A Kolmogorov-Smirnov (K-S) test comparing the two LIRG sub-samples with that of the ULIRG indicates significance levels lower than 1×10^{-5}, implying that it is very unlikely that ULIRGs are drawn from the

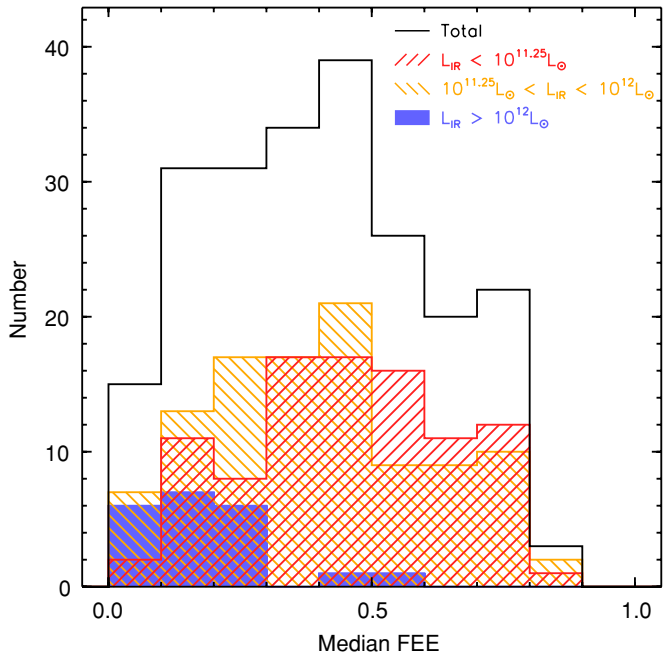

Figure 3. Histogram of the median FEE_{λ} (calculated over the 5–15 μm range) for the GOALS sample (black). The red and orange stripped, and the blue solid histograms are the distributions of the median FEE_{λ} for galaxies with $L_{IR} < 10^{11.25}\,L_{\odot}$, $10^{11.25}\,L_{\odot} \leqslant L_{IR} < 10^{12}\,L_{\odot}$, and $L_{IR} > 10^{12}\,L_{\odot}$, respectively.

(A color version of this figure is available in the online journal.)

same parent distribution as LIRGs. Our data therefore suggest that, as a whole, the median FEE_{λ} of ULIRGs is 2–3 times lower than that of LIRGs.

We now explore whether the spatial extent of the MIR continuum of (U)LIRGs is a smooth function of their IR luminosity or whether there is a certain L_{IR} above which their properties change drastically making their emission substantially more concentrated. The blue circles in Figure 4(a) show the FEE of the 13.2 μm continuum emission ($FEE_{13.2\,\mu m}$) as a function of the L_{IR} for the galaxies in our sample. The size of the circles scales with their distance. As we can see, LIRGs display a wide range of $FEE_{13.2\,\mu m}$. They vary from compact systems ($FEE_{13.2\,\mu m} \simeq 0$) to others which are very extended ($FEE_{13.2\,\mu m} \simeq 0.85$). No clear trend with L_{IR} is evident over the decade in IR luminosity covered by the LIRGs. However, if we examine the median value of the $FEE_{13.2\,\mu m}$ calculated in different luminosity bins (black line), this appears to decrease as the L_{IR} of the galaxies increases, going from $\simeq 0.5$ at $L_{IR} \simeq 10^{10.3}\,L_{\odot}$ to $\simeq 0.1$ at $L_{IR} \simeq 10^{12.3}\,L_{\odot}$. Moreover, for IR luminosities above $\sim 10^{11.8}\,L_{\odot}$, just below the nominal transition between LIRGs and ULIRGs, the maximum of the $FEE_{13.2\,\mu m}$ (upper dashed line) drops abruptly, and only a few galaxies have $FEE_{13.2\,\mu m}$ values larger than 0.2. Indeed, all ULIRGs are unresolved[14] (see Figure 4(b)) and have $FEEs_{13.2\,\mu m} \lesssim 0.2$.

One may consider that the decrease of the median $FEE_{13.2\,\mu m}$ with L_{IR} is due to the loss of spatial resolution (see Figures 4(b) and 1(b)). The more luminous systems tend to be at larger distances and hence their unresolved nuclear component progressively accounts for a larger fraction of their total flux. This bias would affect our ability to measure large values of $FEE_{13.2\,\mu m}$ for distant sources as they become progressively unresolved. We define as unresolved those galaxies whose "core" angular sizes are within 10% of the stellar PSF. We indicate this limit as a dotted line in Figure 4(b). At this point, it is important to differentiate between the core size of a galaxy, used to establish whether it is resolved or not, and its measured FEE. While the former is merely a Gaussian fit to the spatial profile of the nuclear emission of a galaxy from which an FWHM is obtained, the latter also accounts for possible low surface brightness emission which is probably more extended than the core of the galaxy. As a consequence, sources classified as unresolved in Figure 4(b) may still display non-zero $FEE_{13.2\,\mu m}$ values in Figure 4(a).

If our ability to measure the FEE and the size of the MIR emitting region of the galaxies were totally dominated by the instrumental resolution, the fraction of unresolved sources would be a monotonically increasing linear function of distance. To examine this, we divided our sample in three distance bins at [25–75], [75–125], and [150–250] Mpc, each doubling the distance of the previous one, and calculated the fraction of unresolved sources in each one. We find that the corresponding fraction of unresolved sources is 16% (9/55), 33% (29/88), and 45% (18/40). That is, as the distance doubles, the fraction of unresolved sources nearly doubles. However, there are sources up to $\simeq$240 Mpc, for which we can measure a $FEEs_{13.2\,\mu m} \simeq 0.7$ independently of their L_{IR}, implying that we are still able to resolve the EE at those distances if present.

Hence, the steep drop of the maximum value of $FEE_{13.2\,\mu m}$ above $L_{IR} \sim 10^{11.8}\,L_{\odot}$ cannot be explained by a progressive increasing of the distance to the galaxies. We note that all 10 ULIRGs found at distances up to 200 Mpc, where we are still able to measure large values of $FEE_{13.2\,\mu m}$, are unresolved and display $FEEs_{13.2\,\mu m} < 0.2$ (see Figure 4(b)). However, 68% (54/80) of LIRGs at similar distances, between 100 and 200 Mpc are resolved and have large $FEEs_{13.2\,\mu m}$ reaching values up to 0.7. If ULIRGs were drawn from the same parent population as LIRGs, one would expect to resolve around six out of these 10 ULIRGs, which is not the case. Therefore, it appears that there is a real threshold in the distribution of the compactness of IR bright galaxies happening at $L_{IR} \sim 10^{11.8}\,L_{\odot}$, with higher luminosity systems being more compact.

When we examine only the LIRGs of our sample, we find that, independently of the distance, there are systems with more than 50% of their MIR continuum emission originating outside the unresolved central region. This implies that the EE in these systems is larger than the contribution of the unresolved nuclear region to their total MIR luminosity. In fact, we are able to resolve sizes (FWHMs) of LIRG cores up to $\sim$10 kpc, much larger than the spatial resolution at any given distance. However, to ascertain a representative physical size for the sources in a given luminosity range is quite challenging since our sample is flux limited rather than distance limited. Both the FEE and the size of a source depend on whether we can resolve their emission. The resolution though is a function of the distance, and at the same time more luminous galaxies are seen at larger distances. Hence, upper limits on the sizes of sources also depend on their luminosities. If we simply compute the mean core size of LIRGs using only those systems that are resolved, which are those found above the dotted line in Figure 4(b), the result is 3.1 kpc, while the median is 2.7 kpc. A more thorough analysis can be performed using the survival analysis package

[14] There are three systems which deviate from this trend: ESO557-G002, IRAS03359+1523, and IRAS22491-1808. They are interacting systems and their IRAC 8 μm images show the presence of nearby companion galaxies affecting the spatial profiles estimated with the IRS slits. These three systems are marked with green boxes in Figures 1(b) and 4, and they are no longer considered in our analysis.

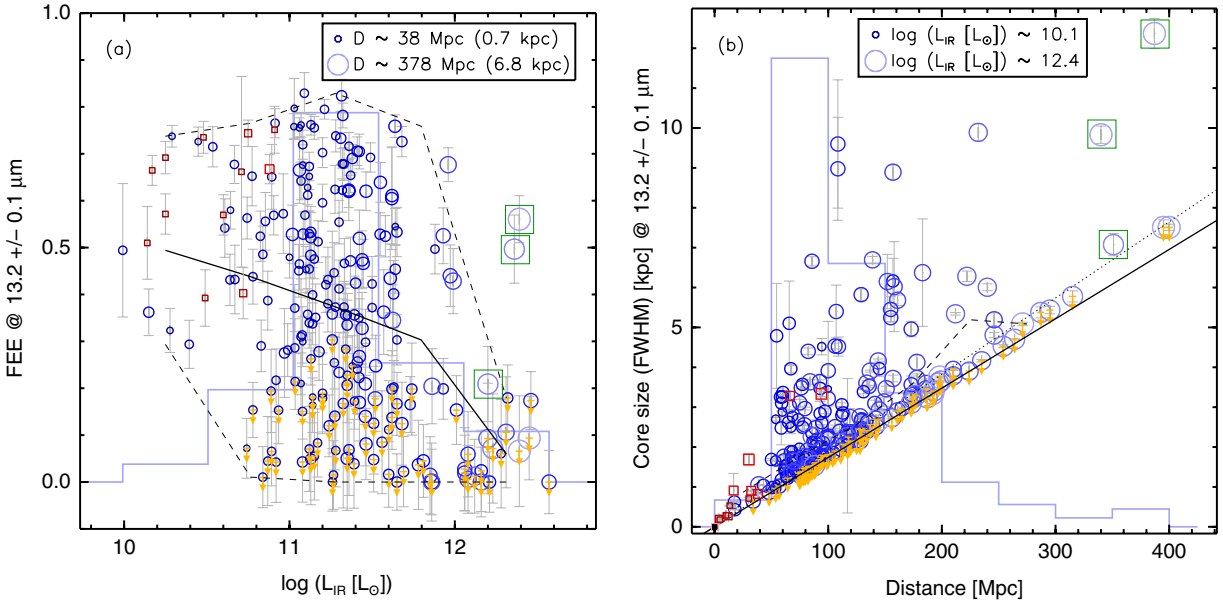

Figure 4. (a) Plot of the FEE of the continuum at 13.2 μm as a function of the IR luminosity for the galaxies of our sample (blue circles). The size of the circles scales with the distance to the galaxy. The red squares in the left and right panels are the results obtained for a sub-sample of galaxies taken from the starburst sample of Brandl et al. (2006, see the text for details). The size of the squares also scales with distance. For reference, the projected linear size of the unresolved component at the given distance is shown in parentheses. The background faint (blue) line is a normalized histogram of the galaxies at different IR luminosity bins. The solid (black) line is the median of the $FEE_{13.2\,\mu m}$ at the different luminosity bins. The lower and upper dashed lines are the minimum and maximum $FEE_{13.2\,\mu m}$ at each bin, respectively. The upper limits marked with orange arrows indicate the galaxies whose core sizes are unresolved (see next). (b) Plot of the linear size of the galaxy core, measured as the FWHM of the Gaussian function fitted to the spatial profile at 13.2 μm, as a function of distance (see the text and the Appendix for details). As in (a), the size of the circles and squares scales with the IR luminosity of the source. The faint (blue) line is a normalized histogram of the galaxies at different distance bins. The solid line represents the size of an unresolved source, the FWHM of the stellar PSF, at 13.2 μm as a function of distance. The black dashed line is the median size of galaxies in each distance bin. The black dotted line indicates the expected location of a galaxy with a core size 10% larger than that of the unresolved stellar PSF (solid line). The three systems which deviate from the main trend due to contamination of the MIR profile by a companion galaxy are marked with green boxes (see the text).

(A color version of this figure is available in the online journal.)

ASURV,[15] which properly takes into account the lower and/or upper limits in a given distribution. If we use this approach, we find that the mean core size of LIRGs at 13.2 μm is 2.6 $\pm$ 0.1 kpc.

Regarding the ULIRG sub-sample, establishing a typical size for the region from which their EE originates is even more challenging since all of them are unresolved. If we consider the ULIRGs located up to a distance of $\sim$100 Mpc as the reference, we can estimate an upper limit for their core sizes of $\sim$1.5 kpc, which is agreement with previous findings (e.g., Soifer et al. 2001).

In order to put our results for the GOALS sample in the context of the less luminous but more numerous galaxies of our local universe, we have analyzed the low luminosity sources from the starburst sample of Brandl et al. (2006). We selected galaxies with $L_{IR} \leqslant 10^{11}\,L_{\odot}$ where the IRS slit was well centered on their nuclei (see their Figure 1): IC 342, Mrk 52, NGC 520, NGC 660, NGC 1097, NGC 1222, NGC 3628, NGC 4088, NGC 4676, NGC 4945, NGC 7252, and NGC 7714. Our measurements are plotted as red squares in Figures 4(a) and (b). We find that the $FEE_{13.2\,\mu m}$ of these systems ranges between $\sim$0.4 and 0.8 and is within the values shown by GOALS galaxies with similar IR luminosities. This suggests that the extent of the MIR continuum emission in starburst galaxies and in the low luminosity tail of the GOALS LIRGs is comparable.

Finally, we should mention that our study provides no evidence that LIRGs with small $FEE_{13.2\,\mu m}$ have the highest IR luminosities since the most point-like sources do not appear to be systematically the most luminous in the 5–15 μm range (see also Figure 3). Instead, as mentioned above, all LIRGs show the same scatter in the $FEE_{13.2\,\mu m}$ at any given distance. It is only above the threshold of $L_{IR} \sim 10^{11.8}\,L_{\odot}$ when we observe a significant reduction of the $FEE_{13.2\,\mu m}$ to values $\lesssim$0.2.

3.3. Dependence of the Extended Emission on the Stage of Interaction

We have shown that there is a strong evolution of the compactness of the MIR continuum emission at $L_{IR} \sim 10^{11.8}\,L_{\odot}$. What is the physical process responsible for this? It is known that most ULIRGs are merging systems with clear signs of interactions (e.g., Clements et al. 1996; Murphy et al. 2001). Could it be that the merging processes in (U)LIRGs which drive the material of the galaxies to their nuclei causing massive SF is the same reason that makes them appear more compact in the MIR?

The galaxies in our sample were classified in five stages: (1) no obvious sign of disturbance in their IRAC or *HST* morphologies, or published evidence that the gas is in dynamical equilibrium (i.e., undisturbed circular orbits); (2) early stage, where the galaxies are within 1′ of each other, but little or no morphological disturbance can be observed; (3) the galaxies exhibit bridges, strong disturbance but they do not have a common envelope and each optical disk is relatively intact; (4) the optical disks are completely destroyed but two nuclei can

[15] The package ASURV is available at http://astrostatistics.psu.edu/statcodes/asurv.

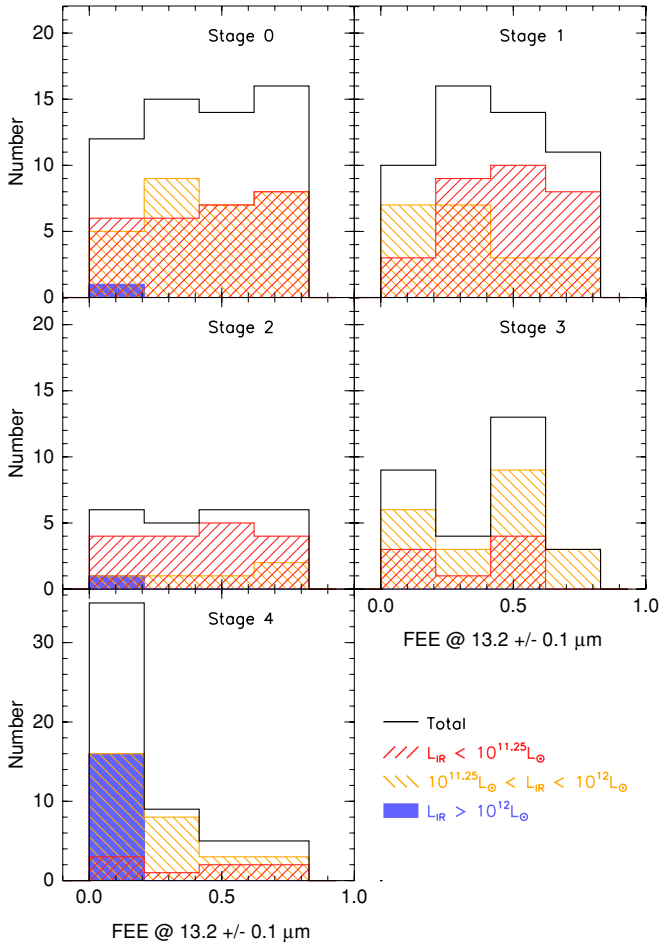

Figure 5. Histograms of the $FEE_{13.2\,\mu m}$ for the galaxies in our sample divided as a function of their merging stage as defined by Petric et al. (2010), from isolated—stage 0—systems, to fully merged—stage 4—galaxies (see Petric et al. 2010, for more details). The galaxies have been separated in different luminosity bins as in Figure 3. We exclude from this analysis the galaxies marked with green boxes in Figure 4 (see Section 3.2).

(A color version of this figure is available in the online journal.)

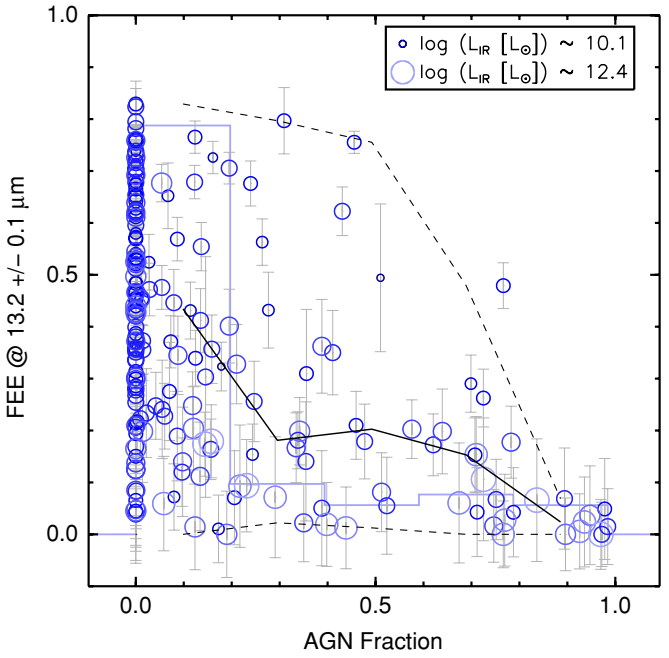

Figure 6. FEE of the 13.2 μm continuum emission as a function of the AGN contribution fraction to the MIR, estimated by the 6.2 μm PAH equivalent width and the MIR continuum emission, for the galaxies of our sample (see Petric et al. 2010). The size of the circles scales with the L_{IR} of the galaxies. The background faint blue line is the normalized histogram of the AGN fraction. The solid black line is the median of the $FEE_{13.2\,\mu m}$ at the different bins of AGN fraction. The lower and upper dashed lines are the minimum and maximum $FEE_{13.2\,\mu m}$ at each bin, respectively.

(A color version of this figure is available in the online journal.)

be distinguished; (5) the two interacting nuclei are merged but structure in the disk indicates the source has gone through a merger. The classification was proposed by Petric et al. (2010) and it is based on *HST* imaging, 3.6 μm *Spitzer* IRAC images as well as optical Sloan Digital Sky Survey (SDSS) images of the sources (see also Surace 1998). In Figure 5, we plot total (black) histograms of the $FEE_{13.2\,\mu m}$ for each interaction stage and also divided in three IR luminosity bins (red, orange, and blue, as in Figure 3). We study 214 (out of the 221) galaxies for which the stage of merger is available. We observe that the most advanced mergers (stage 4) tend to have low $FEE_{13.2\,\mu m}$ values, i.e., they are more compact. K-S tests performed between the total, stage 4 $FEE_{13.2\,\mu m}$ distribution and those of the rest of merging stages yield significance values always lower than 0.01. K-S tests performed among the 0–3 merging stage data sets provide significance values between 0.4 and 0.75. This implies that in fact galaxies classified as to be at merging stage 4 are systematically more compact than those in earlier interaction stages.

Regarding the IR luminosity bin distributions, we see that merging stage 4 systems are not necessarily the most IR luminous only (see also Rigopoulou et al. 1999) but 15% (8/54) have IR luminosities lower than $10^{11.25}\,L_{\odot}$. On the other hand, we find that the vast majority, 89% (16/18), of ULIRGs are systems classified as mergers in their final stage of interaction and all have $FEE_{13.2\,\mu m} \leqslant 0.2$, in agreement with previous findings. Similarly, galaxies at the stage 4 of interaction with $10^{11.25}\,L_{\odot} \leqslant L_{IR} < 10^{12}\,L_{\odot}$ also tend to show lower $FEE_{13.2\,\mu m}$ values (like ULIRGs) than less luminous systems. LIRGs and less IR luminous systems are spread uniformly in the $FEE_{13.2\,\mu m}$ versus L_{IR} parameter space up to the merging stage 2 (the histograms are flat within the uncertainties).

3.4. Extended Emission and Presence of an AGN

Another reason why LIRGs and ULIRGs may appear compact in the MIR is the presence of a dominant AGN. We know that the AGN activity is more prevalent in high IR luminosity systems (e.g., Veilleux et al. 1995, 2009), so we would expect that as the AGN emission starts to dominate the IR energy output of a galaxy, it should appear progressively less extended.

For all galaxies in our sample, the contribution of an AGN to their MIR emission has been estimated by Petric et al. (2010) using a number of line and continuum features. We use their estimates of the AGN contribution fraction to the MIR emission calculated by means of the so-called "Laurent diagram" (Laurent et al. 2000), which is based on the 15 μm/5.5 μm continuum and 6.2 μm PAH/5.5 μm ratios (see Figure 3 of Petric et al. 2010). By comparing the data in this parameter space with representative ratios of pure AGN, PDR, and H II regions, it is possible to infer the contribution of these components to the total galaxy emission. In Figure 6, we present the $FEE_{13.2\,\mu m}$ as a function of this AGN fraction for the 210 galaxies for which it could be derived. The galaxies are again displayed as circles, the size of which scales with their IR luminosity. It

is clear that as the AGN contribution to the MIR approaches unity, the maximum $FEE_{13.2\,\mu m}$ at the different AGN-fraction bins (upper dashed line) decreases and the galaxies become progressively more compact. In addition, the median $FEE_{13.2\,\mu m}$ (solid line) also decreases as the AGN fraction increases, although more smoothly. In fact, only 5 out of the 30 AGN-dominated galaxies[16] have $FEE_{13.2\,\mu m} > 0.2$. Independently of the L_{IR}, it is interesting to see that 60% (15/25) of the AGN-dominated galaxies with $FEE_{13.2\,\mu m} \leqslant 0.2$ are in the final stage of interaction, while only 12% (3/25) are in the third, 0 in the second, 20% (5/25) in the first, and 8% (2/25) in the zeroth (see Figure 5).

We have found that galaxies classified as mergers in their final stage of interaction tend to have low $FEE_{13.2\,\mu m}$ values and, in particular for ULIRGs, $FEE_{13.2\,\mu m} < 0.2$. We also show now that the fraction of ULIRGs in merging stage 4 that are AGN dominated is 60% (9/15). The fraction of galaxies with $10^{11.25}\,L_\odot \leqslant L_{IR} < 10^{12}\,L_\odot$ and $FEE_{13.2\,\mu m} \leqslant 0.2$ (first $FEE_{13.2\,\mu m}$ bin in Figure 5, stage 4) that are AGN dominated is 33% (5/15)[17] while for lower luminosity systems is 33% (1/3). Moreover, the fraction of AGN-dominated galaxies classified as mergers at stage 4 with $FEE_{13.2\,\mu m} > 0.2$ is 0%, independently of the IR luminosity. That is, *all* AGN-dominated galaxies in the stage 4 of interaction are compact.

3.5. Extended Emission and Presence of Cold Dust

Independently of the process that dominates the IR emission in galaxies (either an AGN or a starburst), we should expect to observe harder radiation fields and higher dust temperatures within more compact environments. In this section, we explore whether the EE we detect in the 5–15 μm wavelength range, that traces warm small dust grains and molecules, depends on the amount of cold dust of our sources. We first calculate the *IRAS* $\log(f_{25\,\mu m}/f_{60\,\mu m})$ color of the galaxies, which is a well-known IR broadband AGN diagnostic (de Grijp et al. 1985), but we find that it does not correlate with the extent of the MIR continuum emission. We also explore whether there is a dependence on the *Spitzer* $\log(f_{24\,\mu m}/f_{70\,\mu m})$ and $\log(f_{70\,\mu m}/f_{160\,\mu m})$ colors but do not find any clear trend. However, when we plot in Figure 7 the $FEE_{13.2\,\mu m}$ as a function of the FIR *IRAS* $\log(f_{60\,\mu m}/f_{100\,\mu m})$ color, a correlation is visible. Despite the large scatter, galaxies with cold FIR colors appear to be more extended in their MIR continuum. The Spearman rank correlation coefficient is −0.67 with a significance level of effectively 0, while the Kendall test provides a value of −0.49, implying that the correlation is real. We fitted our data with an outlier-resistant linear fit algorithm provided by the IDL function ROBUST_LINEFIT,[18] and the best-fit parameters are given in the following equation:

$$FEE_{13.2\,\mu m} = 0.04\pm0.02-(1.83\pm0.11)\times\log\left(\frac{f_{60\,\mu m}}{f_{100\,\mu m}}\right), \quad (2)$$

where $FEE_{13.2\,\mu m}$ is the FEE of a given galaxy at 13.2 μm, and $f_{60\,\mu m}$ and $f_{100\,\mu m}$ are the *IRAS* flux densities (f_ν) at 60 and 100 μm, respectively. The data have a scatter of 0.2 in the y-axis and 0.1 in the x-axis. The uncertainties in the parameters of the fit have been calculated using bootstrapping resampling analysis.

[16] We define as AGN-dominated galaxies those that have an AGN contribution fraction to the MIR larger than 0.5.

[17] We have AGN classification for 15 out of 16 galaxies in each of the ULIRG and $10^{11.25}\,L_\odot \leqslant L_{IR} < 10^{12}\,L_\odot$ luminosity bins.

[18] The procedure ROBUST_LINEFIT.PRO can be found in http://spectro.princeton.edu/goddard_doc.html.

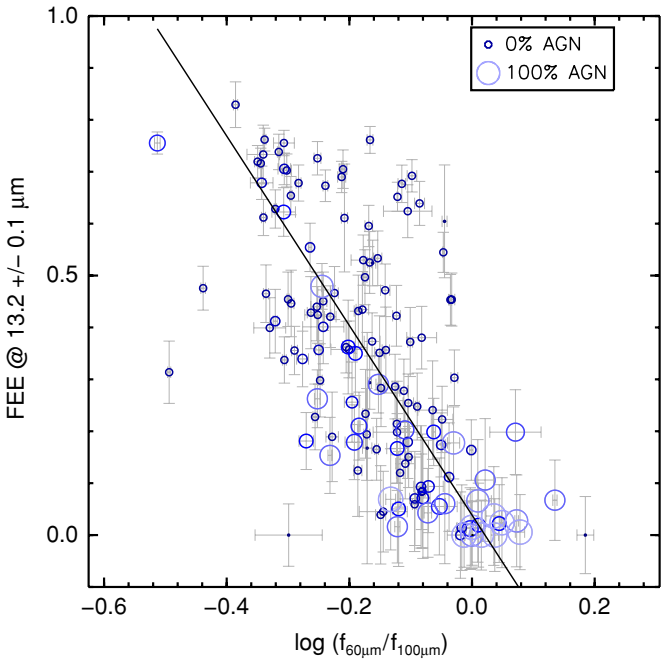

Figure 7. FEE of the 13.2 μm continuum emission as a function of the *IRAS* $\log(f_{60\,\mu m}/f_{100\,\mu m})$ color. The sizes of the circles scale with the AGN fraction of the galaxies. Points indicate galaxies for which the AGN fraction was not available. The solid line is the linear fit to the data.

(A color version of this figure is available in the online journal.)

In order to avoid interacting systems for which only one *IRAS* color has been measured due to its limited spatial resolution, we have used only 142 sources for which there is a unique association between one galaxy (one $FEE_{13.2\,\mu m}$ measurement) and one *IRAS* color. In addition to the correlation, Figure 7 also shows that nearly all galaxies whose MIR emission is dominated by an AGN (i.e., have a high AGN fraction according to the estimates of Petric et al. 2010) are located at the lower right corner of the plot, which means that they are more compact, and have warmer FIR colors. Even if we exclude AGN-dominated systems and consider only starburst galaxies with an AGN fraction close to zero, the correlation is still present.

This result has an interesting implication for the forthcoming studies of the cold dust emission of LIRGs/ULIRGs with the *Herschel Space Telescope*. Figure 7 suggests that "cold" FIR-selected (U)LIRGs will likely present large $FEE_{13.2\,\mu m}$ values. As a result, one would expect that a large fraction of their MIR continuum emission originates in their extended component (see the previous section). Furthermore, based on the study by Bothun & Rogers (1992), the *IRAS* $\log(f_{60\,\mu m}/f_{100\,\mu m})$ colors of our Galaxies suggest that they have very strong dust temperature gradients (their Section 4.1 and Table 3). Consequently the cold, FIR emission from these systems will be more extended than the warmer MIR emission. Taking this into account, the FEE we derive for the MIR continuum emission based on our *Spitzer*/IRS observations places a lower limit to the extent of the FIR continuum emission. Therefore, despite the limitations of our long-slit MIR spectra, one may obtain a rough estimate on how much of the FIR emission is extended in any LIRG/ULIRG.

3.6. Implications For High-redshift SMGs

By virtue of the negative *K*-correction, SMGs are systems with IR luminosities in the ULIRG range, almost independently

of their redshift. Recent studies of SMGs, based on various diagnostics including the MIR and FIR wavelength range, have suggested that they are systems dominated by SF (Pope et al. 2008; Murphy et al. 2009). In addition, interferometric observations of their CO content and radio continuum emission reveal that they host large amounts of dust and molecular gas ($M_{\rm H_2} \sim 10^{10-11}\,M_\odot$) which may fuel prodigious SF rates of several hundred solar masses per year (Neri et al. 2003; Chapman et al. 2004; Greve et al. 2005; Daddi et al. 2009; Tacconi et al. 2008). Analysis of the kinematics of their ionized gas emission using the Hα emission redshifted in the near-infrared indicates that SMGs as well as some high-redshift ULIRGs are extended up to several kpc scales (e.g., Alexander et al. 2010). Taking into account the limits on the spatial resolution of the present day data, some sources display motions which can be attributed to organized rotating disks, and others appear to belong to interacting systems (Tacconi et al. 2008; Bothwell et al. 2010; Ivison et al. 2010). Recent studies of the FIR continuum and [C II] 158 μm emission of high-z IR luminous galaxies also suggest that the SF in these sources is extended over several kpc (Kovács et al. 2010; Hailey-Dunsheath et al. 2010).

It is well accepted that in the local universe the MIR emission traces the SF regions emitting in Hα and correlates with the presence of molecular gas. Based on our analysis, we find no evidence that the local ULIRGs of the GOALS sample are extended in the MIR to the sizes suggested by the Hα or CO measurements of high-z sources. It is true that the *Spitzer* spatial resolution is quite limited, but we have shown that even the closest ULIRGs in our sample have unresolved cores and $\mathrm{FEE}_{13.2\,\mu\mathrm{m}} \lesssim 0.2$. Instead, the LIRG population displays resolved emission extended over several kpc scales, like SMGs.

On the other hand, it is still uncertain whether high-redshift IR luminous sources are simple scaled up analogues of local, less luminous systems in terms of all their physical properties. Integrated MIR spectra of SMGs (Pope et al. 2008; Menéndez-Delmestre et al. 2009) do display PAH equivalent widths more typical of local LIRGs rather than the weaker values found for local ULIRGs (Desai et al. 2007). However, some recent works suggest that the SF law in SMGs is similar to that of local ULIRGs and is much more efficient than in local, less IR luminous disk-like galaxies, or than in high-z BzK galaxies (Daddi et al. 2010a, 2010b; Genzel et al. 2010). We will address the issue of the spectral properties of SF in local LIRGs and ULIRGs in our next paper, where we analyze separately the nuclear and EE of the PAH features, emission lines, and the 9.7 μm silicate feature of the galaxies in the GOALS sample.

4. CONCLUSIONS

We analyzed the spatial profiles of low-resolution 5–15 μm *Spitzer*/IRS spectra of the GOALS galaxy sample and quantified the extent of their MIR emission, FEE_λ. Our work indicates the following.

1. There is a diversity in the shape of the FEE_λ as a function of wavelength. The variation in the spatial extent of the various MIR features such as PAHs, emission lines, and continuum implies that the MIR emission in (U)LIRGs is complex. However, we find three types of FEE_λ functions: constant/featureless, PAH/line extended, and silicate extended. Several physical processes, such as AGN emission as well as multiple bursts of SF, nuclear and extra-nuclear, are suggested to produce the integrated MIR spectrum of (U)LIRGs and to determine their spatial extent at different wavelengths.
2. More than 90% of the galaxies in the GOALS sample have median FEE_λ larger than 0.1. Furthermore, more than 30% of the galaxies have median FEE_λ larger than 0.5, implying that at least half of their MIR emission is extended. As a whole, the median FEE_λ of local LIRGs is ~2–3 times larger than that of ULIRGs.
3. Despite the limited spatial resolution of the *Spitzer*/IRS spectra, we find a steep decrease in the extent of the continuum emission, $\mathrm{FEE}_{13.2\,\mu\mathrm{m}}$, at the threshold of $L_{\rm IR} \sim 10^{11.8}\,L_\odot$. While LIRGs display a wide range of $\mathrm{FEE}_{13.2\,\mu\mathrm{m}}$, spanning from compact objects to sources extended up to 85%, galaxies above this threshold show unresolved cores and very compact emission, in particular ULIRGs, which all have $\mathrm{FEE}_{13.2\,\mu\mathrm{m}} \lesssim 0.2$ independently of their distance. We measure galaxy core sizes (FWHMs) of LIRGs at 13.2 μm up to 10 kpc, with a mean of 2.6 kpc if upper limits to the sizes of unresolved galaxies are taken into account. If only resolved sources are considered, the mean core size of LIRGs is 3.1 kpc. Our estimate for those of ULIRGs is less than 1.5 kpc.
4. As a whole, galaxies classified as mergers in their final stage of interaction, based on imaging from the *Hubble Space Telescope* and *Spitzer Space Telescope*, show lower $\mathrm{FEE}_{13.2\,\mu\mathrm{m}}$ values than galaxies in earlier stages. In terms of IR luminosities, galaxies with $10^{11.25}\,L_\odot \leqslant L_{\rm IR} < 10^{12}\,L_\odot$ in their final stage of interaction display a similar trend (like ULIRGs), showing lower $\mathrm{FEE}_{13.2\,\mu\mathrm{m}}$ values than less luminous systems.
5. The maximum and the median $\mathrm{FEE}_{13.2\,\mu\mathrm{m}}$ decrease as the AGN contribution fraction to the MIR increases. Galaxies with AGN fractions larger than 50% are more compact, and 60% of those that have $\mathrm{FEE}_{13.2\,\mu\mathrm{m}} < 0.2$ are systems in the final stage of interaction. Furthermore, *all* AGN-dominated galaxies classified as mergers in their final stage of interaction have $\mathrm{FEE}_{13.2\,\mu\mathrm{m}} < 0.2$, i.e., are compact, independently of their $L_{\rm IR}$.
6. The $\mathrm{FEE}_{13.2\,\mu\mathrm{m}}$ and the *IRAS* $\log(f_{60\,\mu\mathrm{m}}/f_{100\,\mu\mathrm{m}})$ color appear to be correlated, with the MIR continuum emission of colder galaxies being more extended. Given the large temperature gradients present in our Galaxies, the FEE of the MIR continuum provides a rough lower limit to the FEE of the FIR emission in these systems.

Determining the extent of a galaxy at MIR, FIR, and even radio wavelengths can yield information about how the stellar populations are distributed in it and therefore reveal how the galaxy has formed and evolved. These questions will soon be addressed by new observations obtained with the *Herschel Space Telescope* and the Atacama Large Millimeter Array (ALMA), and in the more distant future with the *James Webb Space Telescope*.

T.D.-S. thanks E. da Cunha for her suggestions and interesting discussions. T.D.-S. and V.C. acknowledge partial support from the EU ToK grant 39965 and FP7-REGPOT 206469. This research has made use of the NASA/IPAC Extragalactic Database (NED), which is operated by the Jet Propulsion Laboratory, California Institute of Technology, under contract with the National Aeronautics and Space Administration, and of NASA's Astrophysics Data System (ADS) abstract service.

APPENDIX

OBTAINING THE FEE$_\lambda$ FUNCTIONS

A.1. Detailed Data Reduction and Calculation of the FEE$_\lambda$

In order to calculate the fraction of extended emission (FEE$_\lambda$) as a function of wavelength, we used as input data the two-dimensional IRS coa2ds files obtained as explained in Petric et al. (2010). Due to the limited spatial resolution of *Spitzer*, we performed the analysis using only the SL module (see Section 2.2), which covers a wavelength range from $\sim$5.5 μm to $\sim$14.5 μm (SL2 order: $\sim$5.5 μm to $\sim$7.5 μm; SL1 order: $\sim$7.5 μm to $\sim$14.5 μm). Details regarding the steps taken for the reduction and creation of the coa2ds can be found in Petric et al. (2010). We used version 18.7 of the *wavesamp* file which contains the information on the projection of the spatial and spectral elements of the IRS slits onto the two-dimensional detector array via a set of pseudo-rectangles. Each pseudo-rectangle defines the spatial direction that crosses an IRS spectrum at a given wavelength. Therefore, to extract the spatial profiles of a galaxy as a function of wavelength, we interpolated the IRS spectrum along the direction traced by each pseudo-rectangle. The same approach was taken to produce the spatial profiles of the standard star used as our reference PSF representing an unresolved source. Each spatial profile was fitted with a Gaussian function leaving as free parameters its maximum intensity, position, and FWHM. Indeed, the latter gives us a measure of the size of the source's "core" at each wavelength (i.e., the Gaussian component of the extended emission; see Figure 4(b)). To calculate the unresolved emission of the galaxy, we scaled the maximum of the PSF spatial profile to the maximum of the galaxy spatial profile and subtracted it. The remaining flux is the EE of the galaxy. We also measured the total emission of the galaxy by integrating the flux over the entire spatial profile defined by the IRS slit. The EE divided by the total emission of the galaxy is the FEE. This calculation was repeated for each wavelength resolution element (pseudo-rectangle) and consequently the FEE is a function of λ (FEE$_\lambda$). The calculation of the FEE$_\lambda$ has some advantages over other methods used to ascertain the compactness of a galaxy, such as the concentration index or the Gini coefficient. The concentration index relies on aperture photometry and therefore does not provide an estimate the shape of the spatial distribution of the PSF, mixing both unresolved and resolved emission. The Gini coefficient is also totally independent of the shape of the galaxy. As a consequence, the growth of the physical size of the unresolved component of the galaxy with distance is not taken into account and it is intrinsically included in the Gini statistics, which would make the interpretation of our results even more challenging.

A.2. Corrections to the FEE$_\lambda$

Since the pixel size of the IRS SL detector is $1\farcs8 \times 1\farcs8$, the IRS spectra are undersampled below $\sim$10 μm. The undersampling affects the spatial distribution of the flux of unresolved sources over the pixels of the detector. As a result, the exact pixel intensity depends on where the source is located on it at a sub-pixel scale. Since an IRS spectrum does not run along the columns of the detector but displays a slight curvature, the spatial profile of the source at each spectral resolution element is not centered at the same sub-pixel position for all wavelengths. Therefore, the undersampling introduces an intrinsic variation on the shape of the spatial profiles as a function of the wavelength, which is reflected in a change of the FWHM as well as the maximum value of the fitted Gaussian to the spatial profiles. The effect of the undersampling can be seen in Figure 8 where the FWHM and maximum of the spatial profiles of the PSF are shown as a function of the wavelength (red lines: top and middle panels). We note that the FWHM and maximum may vary as much as 50% in the SL2 module. This factor is very important because, in order to calculate the amount of EE of a galaxy at a given wavelength, we need to scale the maximum of the PSF to the maximum of the profile of our source. If a galaxy is unresolved, its fitted maximum will present the same behavior as the maximum of the PSF and the wiggling pattern created by the undersampling will cancel out. If, on the contrary, a galaxy is resolved, its spatial profile will not be affected by the undersampling, but the profile of our PSF will be and will introduce this pattern in the calculation of the FEE$_\lambda$.

Therefore, before the calculation of the FEE$_\lambda$ of a galaxy, we need to correct the maximum of the PSF, in a manner which takes into account the undersampling in the spatial profile of the galaxy, which in turn depends on its compactness. In order to calculate how compact the galaxy is, we compare its fitted FWHM with that of the unresolved PSF at each wavelength and correct accordingly the maximum of the PSF. A zero correction means that the galaxy is totally unresolved, as is the PSF. A full correction is applied when the galaxy is much more extended than the PSF and implies that we have to correct the maximum of the PSF as if it was not affected by the undersampling at all. What is this correction factor?

The correction factor to the maximum of the PSF is the value of the FWHM of the PSF normalized to its real value at the same wavelength. This is because even if the FWHM and the maximum of the spatial profile of an unresolved source oscillate as a function of the wavelength due to the undersampling, the total flux does not. As a consequence, the patterns of the FWHM and the maximum of the PSF are "synchronized" (the maximum of one is the minimum of the other; see Figure 8, top and middle panels, red lines) and thus we can use the value of the FWHM to correct the maximum to its real value. In this we assume that the "real" (highest) spatial resolution that can be achieved at a given wavelength is the one defined by the minimum of the lower envelope showed by the pattern of the FWHM function of the PSF. Values larger than this are affected by the undersampling and cause the FWHM of the spatial profiles to be overestimated and, conversely, the maximum to be underestimated. Therefore, in order to correct for the undersampling, we multiply the maximum of the PSF by the ratio of its observed-to-minimum (real) FWHM. As we mentioned above, this correction depends on how resolved a galaxy is. In unresolved sources, the correction is not necessary, while in very extended galaxies it needs to be fully applied. In order to demonstrate the success and accuracy of the method, in Figure 8 we show the FWHM, maximum, and FEE$_\lambda$ function of three galaxies resolved in a different degree. The final FEE$_\lambda$ at a given wavelength is the average of the values obtained for each one of the two nod positions of the IRS slits, and the uncertainty is the difference between both.

We can see that the FEE$_\lambda$ function (bottom panel, green line), once corrected for the undersampling effect, shows almost no residuals of the wiggling pattern that can be seen in the FWHM and maximum functions (top and middle panels) of the galaxies and the PSF. Furthermore, the correction works very well for almost unresolved sources (left panels), very extended sources (right panels), as well as for intermediate-

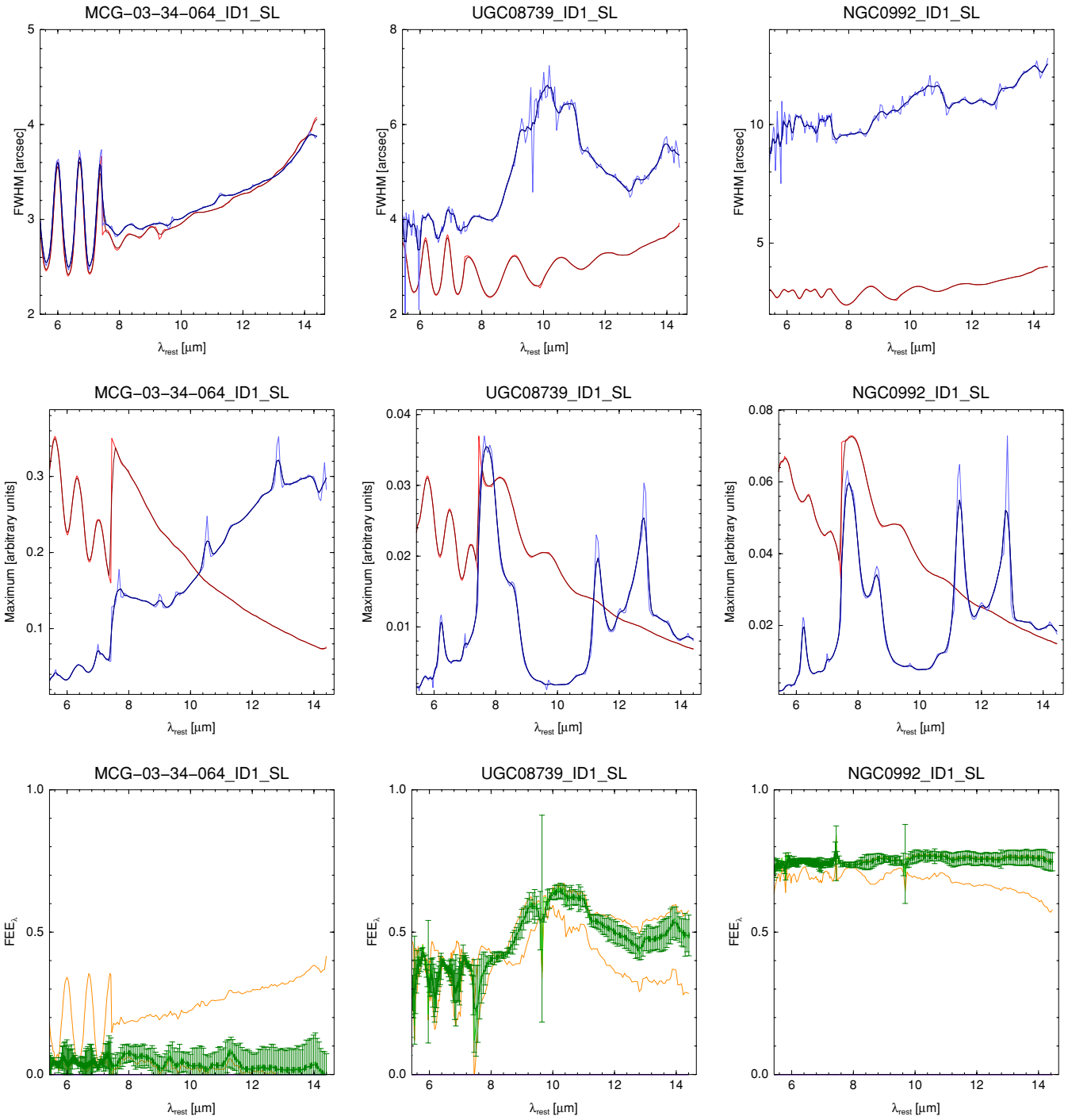

Figure 8. Top panel: FWHM of the Gaussian function for three galaxies of the sample as a function of wavelength and averaged for the two nod positions (blue lines). The FWHM of the PSF is also shown for reference (red lines). The galaxy on the left is unresolved while the other two show FWHMs larger than those of the PSF. Middle panel: maximum of the Gaussian function (arbitrary scaled) for the same three galaxies as a function of wavelength and averaged for the two nod positions (blue lines). These plots are equivalent to the spectra of the galaxies, except that they are affected by the undersampling. The maximum of the PSF (arbitrary scaled at each order) is also plotted for reference (red lines). Bottom panel: fraction of extended emission, FEE$_\lambda$, for the same three galaxies as a function of the wavelength and averaged for the two nod positions (green lines). The bottom orange lines represent the FEE$_\lambda$ that would be obtained if the correction factor was not applied at all, that is, if we considered that the source is totally unresolved. The top orange lines represent the FEE$_\lambda$ that would be obtained if the correction factor was fully applied, that is, if we considered that the source is very extended. See the text for details. The thin-colored lines are actual values. The thick-colored lines are the same values but smoothed with a four-pixel box to reduce the noise.

(A color version of this figure is available in the online journal.)

resolved sources (center panels). As an example, we show in the bottom panels, together with the FEE$_\lambda$ function (in green), the FEE$_\lambda$ function that would have been obtained if we had not applied the correction factor at all (lower orange line) or if it had been fully applied (top orange line), that is if we had not taken into account the a priori knowledge on how extended our Galaxy is. The comparison of the FWHMs of the galaxy and the PSF is therefore essential in order to know to which extent the

correction factor must be applied at a given wavelength. This is specially true for galaxies that are slightly resolved at certain wavelengths, as is the case of UGC 08739 (middle panel).

There were a few cases, however, where an accurate FEE_{λ} function could not be accurately recovered for the SL2 order (IC 4734, ESO 279-G011, MCG-02-33-098, CGCG 468-002, and MCG-05-12-006). These are galaxies that show FWHM functions that do not present a wiggling pattern despite the fact they are almost unresolved. Therefore, their FEE_{λ} functions from $\sim$5.5 μm to $\sim$7.5 μm are very uncertain.

A.3. Additional Tests

In addition, we checked whether the FEE as a function of the wavelength obtained with the IRS spectra is consistent with the value that can be calculated from the IRAC images at 8 μm. To do so we performed a PSF-fitting analysis to the images in the same way as we did for the spatial profiles of the IRS spectra at each wavelength. First, we used a sub-sampled point response function (PRF) for the 8 μm IRAC bandpass provided by the SSC and interpolated it to the sub-pixel position in the image where the galaxy was located. Then, we rebinned the PRF to the pixel size of the IRAC mosaic, scaled it to the peak of the emission of the galaxy, and subtracted the unresolved emission represented by this scaled PRF. Finally, we measured the remaining flux in an area approximately equal to that used for measuring the integrated emission of the galaxy in the IRS slit (see Section 2.4). Using Equation (1) as for the spectroscopy, the $FEE_{8\,\mu m}$ obtained from the IRAC 8 μm imaging is the ratio of the remaining emission to the total integrated emission of the galaxy measured in the same aperture.

There are some cases where the $FEE_{8\,\mu m}$ is greater than the FEE calculated from the IRS spectra. This is due to the different surfaces used for measuring the emission of the galaxy in each case (for imaging and spectroscopy). Although both apertures have the same area, the former has the shape of a box while the one of the IRS slit is very elongated. Since, as it is said above, the slit was not oriented in a preferred direction over the galaxies, a boxy-shaped aperture used for measuring the emission will generally lead to a higher FEE because of its symmetry around the central region of the galaxy which in many cases is axisymmetric. Therefore, the fact that the $FEE_{8\,\mu m}$ is slightly above those calculated using the IRS data for some galaxies is totally consistent with the approach taken and shows that both calculations of the FEE, using imaging and spectroscopy, are in agreement.

REFERENCES

Alexander, D. M., Swinbank, A. M., Smail, I., McDermid, R., & Nesvadba, N. P. H. 2010, MNRAS, 402, 2211
Armus, L., et al. 2007, ApJ, 656, 148
Armus, L., et al. 2009, PASP, 121, 559
Bothun, G. D., & Rogers, C. 1992, AJ, 103, 1484
Bothwell, M. S., et al. 2010, MNRAS, 405, 219
Brandl, B. R., et al. 2006, ApJ, 653, 1129
Bryant, P. M., & Scoville, N. Z. 1999, AJ, 117, 2632
Caputi, K. I., et al. 2007, ApJ, 660, 97
Chapman, S. C., Smail, I., Windhorst, R., Muxlow, T., & Ivison, R. J. 2004, ApJ, 611, 732
Clements, D. L., Sutherland, W. J., McMahon, R. G., & Saunders, W. 1996, MNRAS, 279, 477
Daddi, E., et al. 2009, ApJ, 694, 1517
Daddi, E., et al. 2010a, ApJ, 713, 686
Daddi, E., et al. 2010b, ApJ, 714, L118
de Grijp, M. H. K., Miley, G. K., Lub, J., & de Jong, T. 1985, Nature, 314, 240
Desai, V., et al. 2007, ApJ, 669, 810
Díaz-Santos, T., Alonso-Herrero, A., Colina, L., Packham, C., Levenson, N. A., Pereira-Santaella, M., Roche, P. F., & Telesco, C. M. 2010, ApJ, 711, 328
Díaz-Santos, T., Alonso-Herrero, A., Colina, L., Packham, C., Radomski, J. T., & Telesco, C. M. 2008, ApJ, 685, 211
Downes, D., & Solomon, P. M. 1998, ApJ, 507, 615
Fazio, G. G., et al. 2004, ApJS, 154, 10
Genzel, R., et al. 2010, MNRAS, 407, 2091
Greve, T. R., et al. 2005, MNRAS, 359, 1165
Haan, S., et al. 2010, ApJ, submitted
Hailey-Dunsheath, S., Nikola, T., Stacey, G. J., Oberst, T. E., Parshley, S. C., Benford, D. J., Staguhn, J. G., & Tucker, C. E. 2010, ApJ, 714, L162
Houck, J. R., et al. 1984, ApJ, 278, L63
Houck, J. R., et al. 2004, ApJS, 154, 18
Houck, J. R., et al. 2005, ApJ, 622, L105
Imanishi, M., Nakagawa, T., Ohyama, Y., Shirahata, M., Wada, T., Onaka, T., & Oi, N. 2008, PASJ, 60, 489
Ivison, R. J., Smail, I., Papadopoulos, P. P., Wold, I., Richard, J., Swinbank, A. M., Kneib, J., & Owen, F. N. 2010, MNRAS, 404, 198
Kovács, A., et al. 2010, ApJ, 717, 29
Laurent, O., Mirabel, I. F., Charmandaris, V., Gallais, P., Madden, S. C., Sauvage, M., Vigroux, L., & Cesarsky, C. 2000, A&A, 359, 887
Le Floc'h, E., Charmandaris, V., Laurent, O., Mirabel, I. F., Gallais, P., Sauvage, M., Vigroux, L., & Cesarsky, C. 2002, A&A, 391, 417
Le Floc'h, E., et al. 2005, ApJ, 632, 169
Menéndez-Delmestre, K., et al. 2009, ApJ, 699, 667
Murphy, E. J., Chary, R., Alexander, D. M., Dickinson, M., Magnelli, B., Morrison, G., Pope, A., & Teplitz, H. I. 2009, ApJ, 698, 1380
Murphy, T. W., Jr., Soifer, B. T., Matthews, K., & Armus, L. 2001, ApJ, 559, 201
Neri, R., et al. 2003, ApJ, 597, L113
Pereira-Santaella, M., et al. 2010, ApJS, 188, 447
Pérez-González, P. G., et al. 2005, ApJ, 630, 82
Petric, A. O., et al. 2010, ApJ, submitted
Pope, A., et al. 2008, ApJ, 675, 1171
Rieke, G. H., et al. 2004, ApJS, 154, 25
Rigby, J. R., et al. 2008, ApJ, 675, 262
Rigopoulou, D., Spoon, H. W. W., Genzel, R., Lutz, D., Moorwood, A. F. M., & Tran, Q. D. 1999, AJ, 118, 2625
Sanders, D. B., Mazzarella, J. M., Kim, D.-C., Surace, J. A., & Soifer, B. T. 2003, AJ, 126, 1607
Sanders, D. B., & Mirabel, I. F. 1996, ARA&A, 34, 749
Soifer, B. T., & Neugebauer, G. 1991, AJ, 101, 354
Soifer, B. T., et al. 2000, AJ, 119, 509
Soifer, B. T., et al. 2001, AJ, 122, 1213
Spoon, H. W. W., et al. 2004, ApJS, 154, 184
Surace, J. A. 1998, PhD thesis, Univ. Hawaii
Tacconi, L. J., et al. 2008, ApJ, 680, 246
Veilleux, S., Kim, D.-C., Sanders, D. B., Mazzarella, J. M., & Soifer, B. T. 1995, ApJS, 98, 171
Veilleux, S., et al. 2009, ApJS, 182, 628
Werner, M. W., et al. 2004, ApJS, 154, 1
Yan, L., et al. 2005, ApJ, 628, 604